ChemPubSoc Europe

DOI: 10.1002/batt.201900140

BATTERIES & SUPERCAPS
Articles

Special Collection

Deriving Structure-Performance Relations of Chemically Modified Chitosan Binders for Sustainable High-Voltage $LiNi_{0.5}Mn_{1.5}O_4$ Cathodes

Matthias Kuenzel,[a, b] Regis Porhiel,[a, b] Dominic Bresser,*[a, b] Jakob Asenbauer,[a, b] Peter Axmann,[c] Margret Wohlfahrt-Mehrens,[a, c] and Stefano Passerini*[a, b]

The implementation of aqueous electrode processing for lithium-ion positive electrodes is key towards the realization of environmentally benign and cheap battery production. One of the water-soluble binders that has attracted most attention is chitosan, the second-most abundant natural biopolymer. Herein, the use of chitosan for high-voltage, cobalt-free $LiNi_{0.5}Mn_{1.5}O_4$ cathodes is reported for the first time. A detailed comparison of three different grades of chitosan with varying chain length and degrees of deacetylation (DD) is provided to explore the impact of these properties on the electrochemical performance. In fact, bio-derived chitosan with a relatively lower DD outperforms synthetic chitosan-especially after crosslinking with citric acid-yielding about 10% higher capacities. Higher molecular weight appears additionally advantageous for the cycling stability. Finally, guar gum is employed as slurry thickener, co-crosslinking with chitosan. This allows for achieving 50% higher mass loadings than for chitosan only and stable capacities above 130 and 120 mAh g^{-1} at C/3 and 1 C, respectively.

1. Introduction

Shortly after their market introduction by Sony in 1991, rechargeable lithium-ion batteries have rapidly superseded long-established systems, such as Ni–MH and Ni–Cd, to become the dominant energy storage technology for portable electronic devices.[1,2] Considering their tremendous success over the past 28 years and in sight of the announcement of several car manufacturers across Europe, Asia and the US to completely electrify their fleet in the near future, it appears reasonable to expect another leap forward in battery market growth within the next (half) decade.[3–7] This, however, is raising interests toward a more sustainable battery production,[8,9] eventually eliminating the use of non-abundant and toxic raw materials, i.e., cobalt.[10,11] In addition, the development of environmentally benign electrode processing technologies based on natural and cheap binders and water as the dispersion agent and solvent is rapidly emerging.[12,13] The search for alternative binders, allowing for the implementation of water as a replacement of toxic *N*-methylpyrrolidone (NMP),[14–16] which is required for the use of mutagenic and teratogenic polyvinylidene difluoride (PVdF)[17] as binder, has stimulated the creativity and inventiveness of researchers worldwide. The new systems proposed include inter alia water/ethanol-processable polymers (e.g., fluoroacrylic polymers, TRD 202a),[18,19] fluorine-free macromolecules (e.g., poly(acrylic acid), PAA[20–22] and poly(vinyl acetate), PVA),[23,24] as well as bio-derived polymers (e.g., alginates[25–27] and their derivatives like carboxymethyl cellulose, CMC).[28–30] Among these, chitosan, the deacetylated derivative of chitin, is the second-most abundant natural polymer after cellulose. Chitin is available in large quantities as shell waste from commercial farming of shrimps, lobsters and crabs, thus, being a cheap and readily available source for carbohydrate-based long-chain polymers with *N*-acetyl substituents along a glucosamine backbone.[31] The deacetylation is conducted by a facile heat treatment (90~120 °C) in an aqueous NaOH solution (4~5 h), yielding chitosan as a copolymer of β-(1,4)-linked *N*-acetyl-D-glucosamine and D-glucosamine units, while the final degree of deacetylation (DD) depends on the eventual experimental conditions.[32] The D-glucosamine moiety is subsequently protonated by weak organic acids, e.g., diluted acetic acid, to render the copolymer water-soluble and receptive for potential crosslinking reactions using, for instance, carboxylic acids or aldehydes.[31,33] Following such an approach, Gao et al.[34] employed glutaraldehyde to crosslink the chains of chitosan, yielding antimony-based, composite negative electrodes, which exhibited better cycling stability and electrode integrity in Na-ion batteries compared to those employing the non-crosslinked binder. However, glutaraldehyde is highly toxic and very harmful to aquatic life

[a] M. Kuenzel, R. Porhiel, Dr. D. Bresser, J. Asenbauer, Dr. M. Wohlfahrt-Mehrens, Prof. S. Passerini
Helmholtz Institute Ulm (HIU),
Helmholtzstrasse 11, 89081 Ulm, Germany
E-mail: dominic.bresser@kit.edu
stefano.passerini@kit.edu
[b] M. Kuenzel, R. Porhiel, Dr. D. Bresser, J. Asenbauer, Prof. S. Passerini
Karlsruhe Institute of Technology (KIT),
P.O. Box 3640, 76021 Karlsruhe, Germany
[c] Dr. P. Axmann, Dr. M. Wohlfahrt-Mehrens
Zentrum für Sonnenenergie- und Wasserstoff-Forschung Baden-Württemberg (ZSW),
Helmholtzstrasse 8, 89081 Ulm, Germany

Supporting information for this article is available on the WWW under https://doi.org/10.1002/batt.201900140

Special Collection An invited contribution to a Special Collection dedicated to the Symposium on Batteries and Supercapacitors at the E-MRS Spring Meeting 2019

with long-lasting effects on the environment. Thus, it does not qualify as a crosslinker of environmentally benign binders for sustainable lithium-ion battery production.[35] Therefore, other molecules, such as polyacrylic acid (PAA) and citric acid (CA), known from different branches of metal recovery and wood industry,[36,37] have recently been adapted for silicon/graphite composite electrodes for lithium-ion batteries. These have led to an improved chitosan-based binder after carefully adjusting the ratios of PAA, chitosan, CA, and the acetic acid necessary for dissolving chitosan in water.[38] Although the resulting electrodes displayed higher first cycle coulombic efficiency and better cycling stability over 50 cycles, ascribed to the higher tensile strength introduced by the citric acid crosslinking, the authors mentioned that it would not be possible to remove the acetic acid contamination from the electrode slurry.[37,38] This certainly has an impact on the final electrode's mechanical and electrochemical properties since the acetic acid possibly binds to the deacetylated glucosamine units of chitosan, but is too short for bridging the chitosan chains. This might eventually result in the formation of side chains and branched polymers rather than true crosslinking. At least as important with respect to the implementation of such binder systems for Co-free positive electrode materials like high-voltage spinel $LiNi_{0.5}Mn_{1.5}O_4$ (LNMO) is the sensitivity of these compounds towards the electrode slurry pH due to the need of adding mild organic acids to dissolve chitosan.[39–42] In fact, LNMO is very prone to acid-promoted dissolution of transition metals and lithium ions in aqueous solution. It is presumably for this reason that pure chitosan without chemical modification, such as carboxymethylation,[43,44] has so far not been reported as a binder for LNMO and other kinds of oxide-based positive electrode materials for LIBs.[45,46]

Herein, it is demonstrated that (CA-crosslinked) chitosan can be employed as binder also for high-voltage LNMO cathodes when incorporating minor amounts of phosphoric acid. The latter has been earlier reported as effective inhibitor for the aluminum current collector corrosion and electrode/electrolyte interface stabilization agent.[25,47–49] In contrast to mild organic acids, PA has no negative-in fact, rather a positive-impact on the electrochemical performance of oxide-based positive electrode materials. In addition, the influence of different degree of deacetylation and molecular weight of the chitosan polymer along with the CA-induced crosslinking on the mechanical and electrochemical properties of the resulting electrodes is investigated. Eventually, guar gum is introduced as a more flexible polymer to obtain a co-crosslinked polymer blend further improving the best-performing chitosan-based LNMO electrodes.

Table 1. Overview of some general properties of the investigated chitosan samples and the herein used abbreviation for the different samples.

Sample & property	Chitosan-99, low M_w	Chitosan-85, low M_w	Chitosan-75, high M_w
Source of Chitin	synthetic	bio-derived	bio-derived
Ø Molecular weight	100 kDa	50–190 kDa	310–375 kDa
Specified Viscosity (1 wt.% in dilute (1 %) acetic acid)	< 10 cP	20–300 cP	800–2000 cP
Solubility in H_2O at RT	insoluble	insoluble	slightly soluble
Degree of Deacetylation (DD)	> 99 %	~ 85 %	~ 75 %
Abbreviation for citric acid crosslinking	Chi-99-X, low M_w	Chi-85-X, low M_w	Chi-75-X, high M_w
Abbreviation for the Guar Gum blend	–	–	Chi-75-X-GG

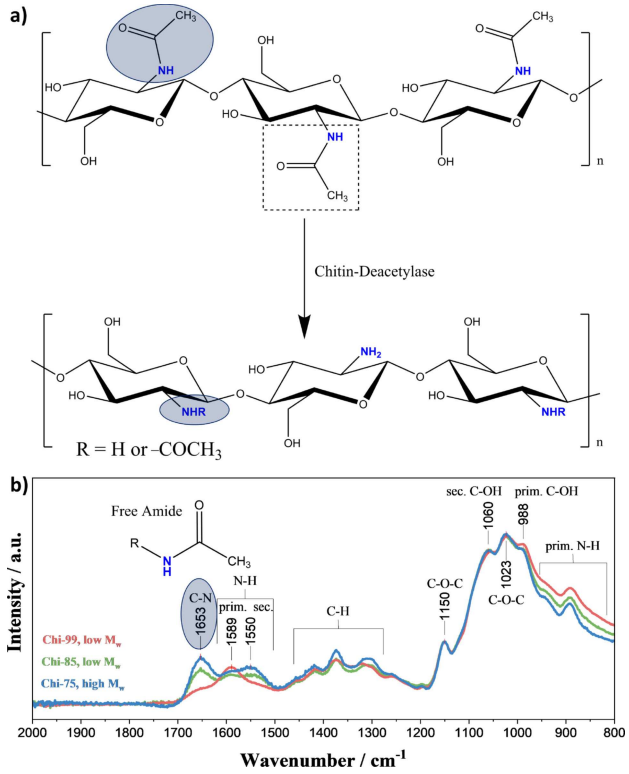

Figure 1. (a) Scheme for the production of chitosan via enzyme-catalyzed deacetylation of chitin. (b) FTIR spectra of three chitosan samples with different DD and molecular weight (M_w). Chi-75 (blue; ~ 75 % DD; high M_w ~ 350 kDa) Chi-85 (green; ~ 85 % DD; low M_w ~ 100 kDa), and Chi-99 (red; 99 % DD; low M_w 100 kDa).

Experimental Section

Structural and Morphological Characterization

The active material, $LiNi_{0.5}Mn_{1.5}O_4$ (LNMO; d50 = 14.4 µm; BET surface area: < 1.0 $m^2 g^{-1}$; tap density = 2.26 g cm^{-3}), was prepared in a continuously-stirred tank reactor according to the co-precipitation method and temperature treatment to tune particle size and morphology for high-voltage applications described by Axmann *et al.*[50] Scanning electron microscopy (SEM) analysis of the as-prepared composite cathode tapes was performed on a Zeiss Crossbeam 340 field-emission electron microscope. The FTIR measurements were carried out on a Vertex 70v IR spectrometer (Bruker) equipped with a MIR light source, KBr beam splitter and a deuterated L-alanine-doped triglycine sulfate (DLaTGS) detector with a KBr window. The single reflection diamond attenuated total reflection accessory (PLATINUM ATR from Bruker) was employed for the IR-ATR measurements. The collected spectra were averaged over 128 scans with an optical resolution of 1 cm^{-1}. The stoichiometry of the LNMO powder was determined through

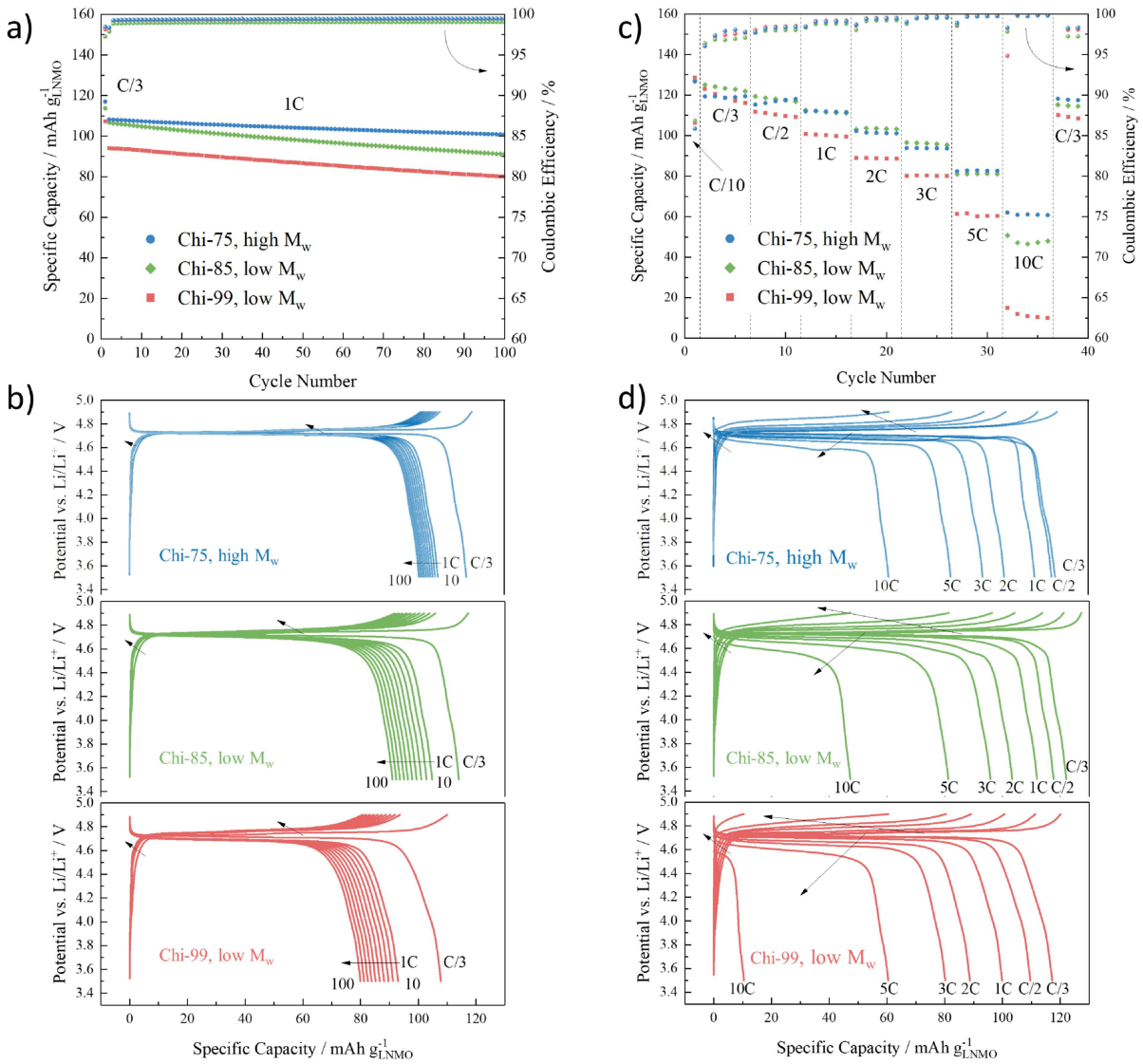

Figure 2. (a) Constant current cycling, and (b) selected potential profiles of LNMO electrodes with the three different chitosan binders of various M_w and DD. (c) Investigation of the rate capability for these electrodes and (d) selected potential profiles for the different C-rates applied. In all cases, the cut-off potentials were set to 3.5 and 4.9 V and a dis-/charge rate of 1 C corresponds to a specific current of 147 mA g^{-1}.

compositional chemical analysis by means of inductively coupled plasma optical emission spectrometry (ICP-OES) utilizing a Spectro Arcos spectrometer (Spectro Analytical Instruments).

Electrode Preparation

The dry electrode composition was 87 wt% LNMO, 10 wt% conductive carbon (C-ENERGY Super C45, IMERYS) and 3 wt% binder. Three different binders were used. Pure chitosan (Chi-Y) with varying molecular weight and a specified DD in Y% (Chi-99, High Purity Chitosan, non-animal derived, average M_w 100 kDa, DD > 99%; Chi-85, Low Molecular Weight Chitosan, M_w 50 ~ 190 kDa, DD 85%; Chi-75, High Molecular Weight Chitosan, M_w 310 ~ 375 kDa, DD 75%; all from Sigma-Aldrich), a 9:1 mixture of Chi-Y and citric acid (CA, 99%, Sigma-Aldrich) or the 1:1:1 blend of Chi-75, natural guar gum (GG, Lamberti SpA) and CA. For the electrode preparation, the binder was dissolved in very diluted phosphoric acid (PA; ortho-phosphoric acid 85%, purity > 99%, Bernd Kraft; 0.3 wt% in deionized water) to obtain a 1.0 wt% binder solution. Subsequently, the conductive carbon and the active material were added to the binder solution. The resulting slurries were homogenized by planetary ball milling for 2 h prior being cast on carbon-coated aluminum foil (thickness: 20 µm; battery grade) utilizing a laboratory doctor blade (wet film thickness of 200 µm). After immediate pre-drying in an atmospheric oven (ED-115, Binder) for 10 min at 80 °C, the electrode tapes were dried at room temperature overnight in the dry room. Disc electrodes (geometric area: 1.13 cm^2) were punched and pressed at 5 tons for 1 min (Atlas manual hydraulic press, Specac) under dry atmosphere. Finally, the electrodes were further dried under vacuum at 120 °C for 16 h. To achieve comparable active material mass loadings for all electrodes, the wet film thickness was adjusted according to the slurry viscosity, ranging from 100 µm to 250 µm. The mass loading of electrodes without guar gum was in the range of 2.7–3.5 mg cm^{-2}. Electrodes employing also guar gum had a higher mass loading in the range of 4.7–4.9 mg cm^{-2}. For the FTIR measurements, suspensions only containing water and a 9:1 mixture of Chi-Y binder and CA were prepared under prolonged stirring (3 days) and mild heating at 60 °C followed by casting on

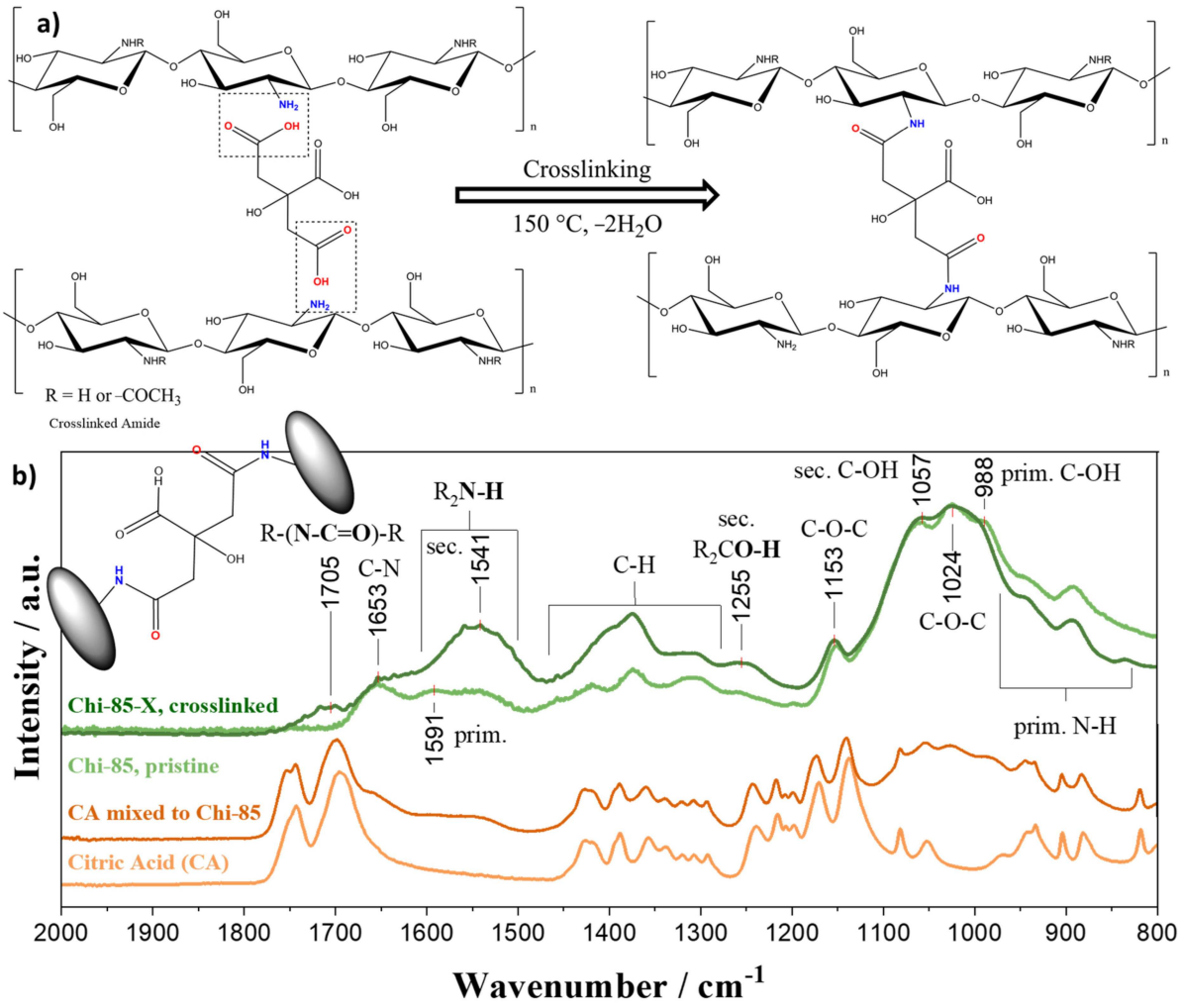

Figure 3. (a) Scheme for the crosslinking reaction via temperature-induced amide condensation of the free chitosan amino groups and citric acid. (b) FTIR spectra of citric acid (light orange), the simple mixture of citric acid and chitosan (Chi-85) without any temperature treatment (dark orange), pure Chi-85 (light green) and citric-acid-crosslinked Chi-85-X (dark green) with the characteristic secondary amine-/amide-related bands arising at 1540–1550 cm^{-1} and 1705 cm^{-1}, respectively, indicating the crosslinking reaction.

Mylar® foil and pre-drying at 80 °C prior to a final drying step at 120 °C.

Electrochemical Characterization

Three-electrode Swagelok cells employing lithium metal foil (thickness 500 µm, battery grade, Honjo Metal) as counter and reference electrodes were used for the electrochemical characterization. The cell assembly was carried out in an argon-filled glove box (MB200B ECO, MBraun; H_2O and O_2 content lower than 0.1 ppm) using glass fiber sheets (Whatman GF/D) as separator. The latter was soaked with 130 µL of electrolyte (1 M $LiPF_6$ in ethylene carbonate (EC)/dimethyl carbonate (DMC), 1:1 w/w, Selectilyte LP 30, BASF). Galvanostatic cycling was performed within a potential range from 3.5 V to 4.9 V at 20 ± 2 °C utilizing a Maccor Battery Tester 4300. An applied dis-/charge rate of 1 C corresponds to a specific current of 147 mA g^{-1}. All potential and voltage values given herein refer to the Li^+/Li quasi-reference redox couple. For each experiment, we investigated at least three, commonly four to five cells to ensure high reproducibility. The error in the reported specific capacities is estimated to be ~1% based on the weighing errors of the balance used for the slurry preparation (± 1.0 mg) and the determination of the active material mass loading of the electrodes (± 0.01 mg).

Results and Discussion

For the reader's convenience, some general physical properties of the chitosan samples investigated herein as well as the corresponding acronyms are summarized in Table 1.

Chitosan can be obtained from chitin at various DDs according to the reaction schematized in Figure 1a. The deacetylation is commonly catalyzed through enzymes or occurs under basic conditions.[31,32] The resulting chitosan powders vary slightly in their chemistry, providing different ratios of –OH and $–NH_2$ functional groups, which affects their solubility and viscosity in the dissolved state and may have an impact on potential crosslinking reactions.[31] The normalized FTIR spectra recorded for the three investigated chitosan samples reveal those differences (Figure 1b): The synthetically derived "pure chitosan" (red trace) with a specified DD > 99%

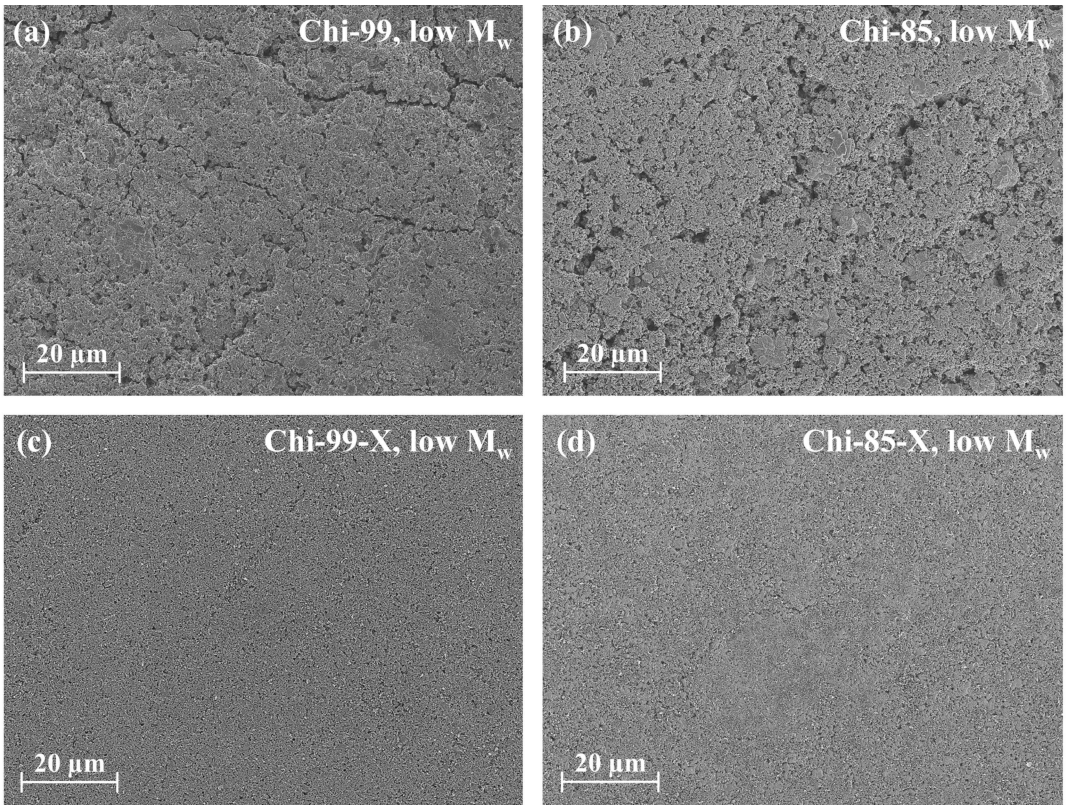

Figure 4. Comparison of SEM micrographs for pressed LNMO electrodes based on low M_w (a) Chi-99 and (b) Chi-85 as binder as well as the CA-crosslinked analogues (c) Chi-99-X and (d) Chi-85-X – all at the same magnification.

shows a well-pronounced peak at 1589 cm^{-1}, corresponding to the N–H deformation vibration of primary amines, and a small shoulder related to the C–N stretching vibration of the free primary acetyl amide (1653 cm^{-1}), which confirm the high DD.[32] In contrast, the chitosan samples of low (green) and high (blue) molecular weight (M_w) have lower DD, 85% and 75%, respectively, as indicated by the higher intensity of the free amide peak located at 1653 cm^{-1}, accompanied by the evolution of the feature corresponding to secondary amines (1550 cm^{-1}). Also, the intensity of the band related to primary amines (1589 cm^{-1}) is relatively reduced as the *N*-acetyl moieties remain prevalent on the chitosan backbone according to the lower DD.[32] At the same time, the features ascribed to the very broad out-of-plane bending vibrations of N–H in primary amines, decrease in the order "Chi-99" (DD > 99%, large amount of primary amines, $-NH_2$), "Chi-85" (DD ~ 85%, medium amount of primary amines, $-NH_2$ and some *N*-acetyl moieties), and "Chi-75" (DD ~ 75%, lower amount of primary amines, $-NH_2$ and more *N*-acetyl moieties).[51]

The electrochemical performance of the LNMO-based electrodes is clearly affected by the type of chitosan used as binder (Figure 2). The comparison of the electrodes' cycling stability in Figure 2a reveals that a very high DD has a detrimental impact on the overall capacity, i.e., LNMO electrodes comprising Chi-99 show a significantly lower capacity than Chi-85 and Chi-75. This inferior performance is essentially ascribed to the large number of free amine groups, which are easily protonated by the phosphoric acid added to facilitate the chitosan dissolution and buffer the slurry pH, stabilizing the cathode interface and preventing lithium and transition metal leaching.[47,48] This latter aspect might be competing with the preferential binding of the phosphate anions to the amine groups and/or the formation of phosphoesters.[25] Also important, when maintaining the electrode preparation comparable, the electrode slurry with Chi-99 shows a rather low viscosity compared to those obtained with lower DD, which may result in the settling of the LNMO particles upon coating and drying. Low viscosity slurries are, in fact, reported to fail in building up the network of conductive particles and active materials bridged by binder strings.[52] Differently, the use of the bio-derived chitosan samples with lower DD (Chi-85 and Chi-75) leads to thicker and more stable slurries. The resulting LNMO electrodes show very similar initial capacity values and very similar coulombic efficiencies of about 99.3–99.4% (Figure 2a). Specifically, the average coulombic efficiency over 100 cycles for Chi-99 was 99.4% compared to 99.3% for Chi-85 and 99.4% for Chi-75, i.e., without any apparent trend concerning the DD or M_W. Nevertheless, the cycling stability is much improved for those electrodes employing the high molecular weight, but low DD chitosan (Chi-75; Figure 2a,b). Generally, the same trend is also observed for the rate capability test (Figure 2c,d), in which the electrodes based on Chi-75 achieve the highest and most stable capacities. Remarkably, however, the electrodes based on Chi-85 show similar capacities up to 5 C, indicating that the

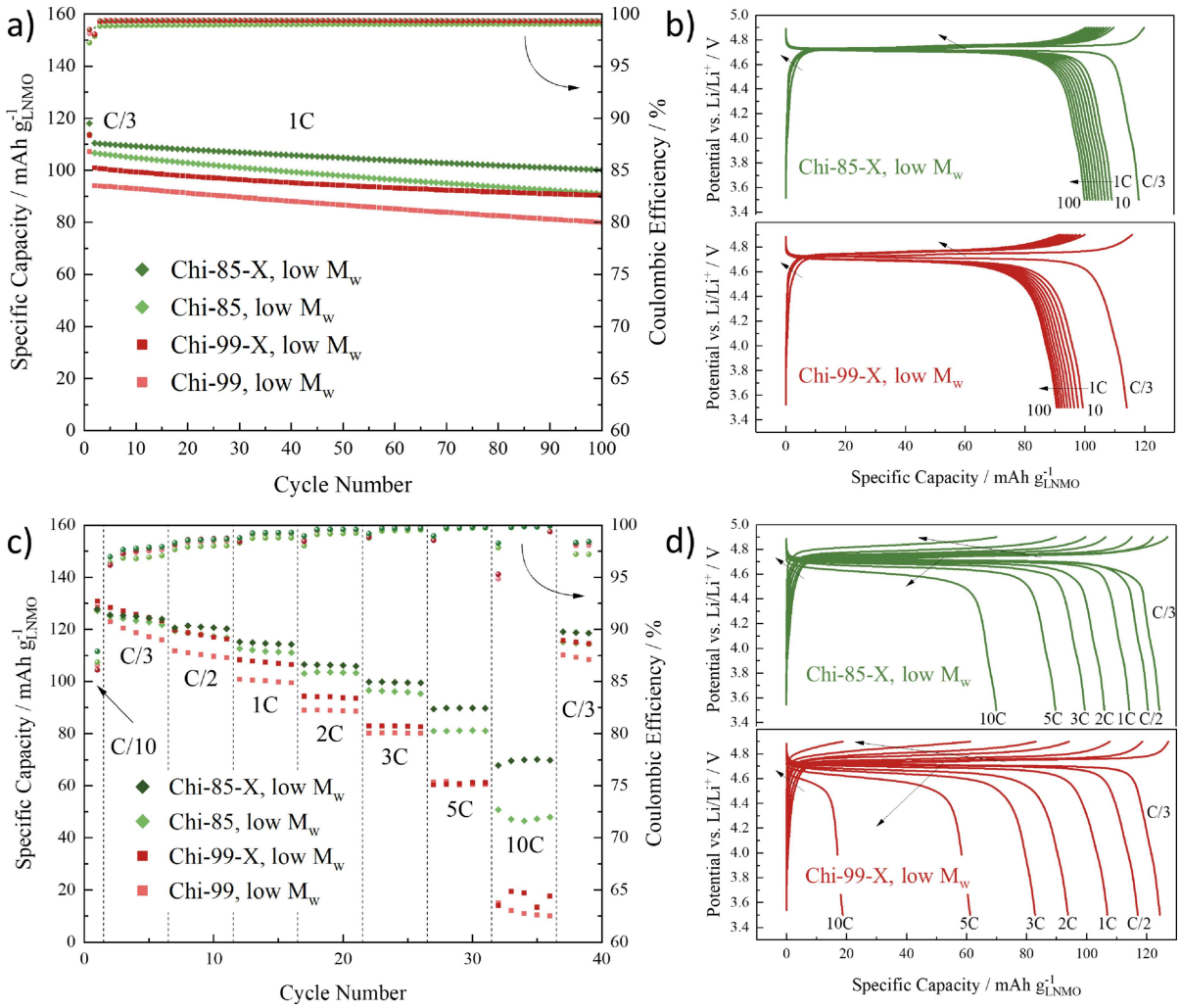

Figure 5. (a) Comparison of the constant current cycling of LNMO electrodes based on low M_w Chi-85 and Chi-99 (light green and light red – both shown already in Figure 2a and herein once again for comparison reasons) as well as their crosslinked analogues Chi-99-X and Chi-85-XX in dark red and dark green, respectively. (b) Selected potential profiles for the crosslinked electrodes Chi-99-X (dark red) and Chi-85-X (dark green). (c) Investigation of the rate capability for the four aforementioned electrode types and (d) selected potential profiles for the crosslinked electrodes at different C rates. In all cases, the cut-off potentials were set to 3.5 and 4.9 V and a dis-/charge rate of 1 C corresponds to a specific current of 147 mA g^{-1}.

capacity fading observed upon constant current cycling (Figure 2a) is not related to inferior kinetics, but rather to the inferior electrode integrity and/or reactivity of the remaining functional groups. For both Chi-75 and Chi-85 based electrodes, the voltage profiles still nicely resolve the weak 'manganese feature' related to the $Mn^{3+/4+}$ couple around 4.0 V – even at high dis-/charge rates of 5 C (Chi-85) and 10 C (Chi-75).[50,53,54] In contrast, the electrodes containing Chi-99 suffer of significant fading when increasing the C rate (Figure 2c) related to the substantial polarization and do not display the 'manganese feature' at elevated dis-/charge rates (Figure 2d). This generally poorer performance is presumably (amongst others) related to the lower slurry viscosity and, thus, less favorable electrode architecture as described earlier.

In order to further improve the electrochemical performance of the chitosan-based electrodes, especially regarding long-term cycling stability, citric acid was employed as processing additive to crosslink the binder in situ upon electrode drying targeting a stabilized electrode coating network. According to the reaction scheme in Figure 3a, the free amine (-NH_2) groups along the chitosan chains can be crosslinked by citric acid via temperature-induced amide condensation.[37,38] A series of comparative FTIR measurements were performed, eventually confirming the proposed mechanism. Exemplarily only the data for Chi-85 are shown, since it is characterized by intermediate M_w and DD values and is, thus, considered the most representative. Figure 3b displays the spectra of pristine Chi-85, citric acid (CA) and the non-crosslinked mixture thereof (i.e., without applying any thermal treatment) for reference. As expected, the latter spectrum resembles the sum of the other two traces after normalization. However, after heat treatment of the film, the spectrum is substantially different. The N–H deformation vibration (1591 cm^{-1}) and out of plane bending (895 cm^{-1}) of primary amines vanishes and decreases in intensity, respectively, while new bands at ca. 1540–1550 cm^{-1} and 1705 cm^{-1}, respectively

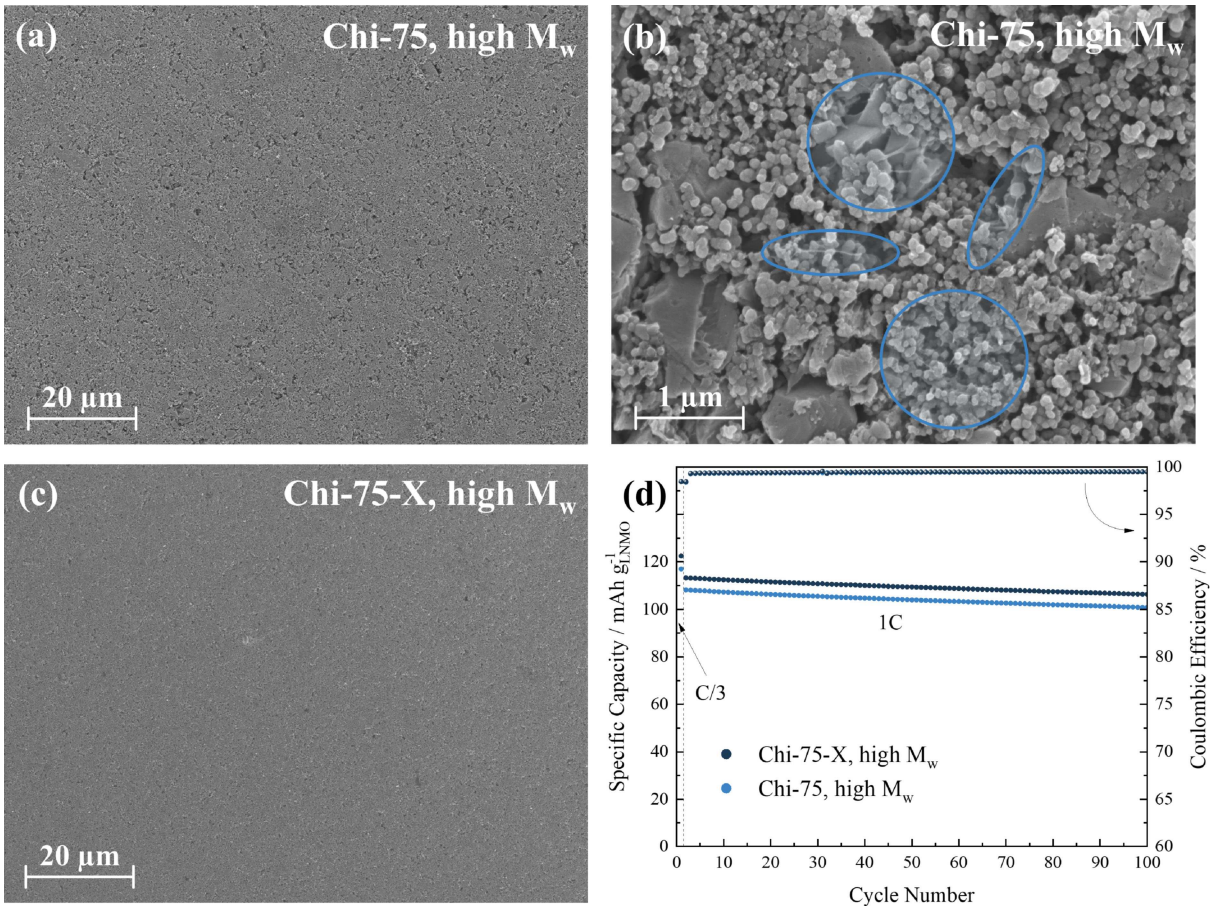

Figure 6. Comparison of SEM micrographs for pressed LNMO electrodes based on high M_w Chi-75 as binder at (a) low and (b) high magnification, as well as the (c) CA-crosslinked analogue Chi-75-X. The blue ellipsoids in (b) highlight the detectable polymer strings interconnecting the electrode components. (d) Comparison of the constant current cycling of LNMO electrodes based on high M_w Chi-75 (light blue-shown already in Figure 2a and herein once again for comparison reasons) as well as after crosslinking with citric acid (Chi-75-X, dark blue).

assigned to secondary amines and the crosslinked secondary amide, appear. These changes further support the condensation-type crosslinking resulting in the chitosan chains being interconnected by CA (see the top left inset in Figure 3b). The FTIR spectra recorded for Chi-99, Chi-75 and their mixtures with CA (before and after the temperature-induced crosslinking) follow the same trend with slightly higher and lower intensities for the new peaks arising in case of Chi-99 and Chi-75, respectively (Figure S1).

The advantage offered by the crosslinking is obvious comparing the SEM micrographs recorded for the pressed LNMO electrodes comprising low M_w Chi-99 and Chi-85 and their CA-crosslinked analogues Chi-99-X and Chi-85-X (Figure 4). While the electrodes based on non-crosslinked Chi-99 and Chi-85 (Figure 4a and Figure 4b, respectively) display a rather rough and porous surface with cracks and defects scattered across the electrode area and penetrating deeply into the electrode coating layer (as exemplarily shown by cross-sectional SEM analysis for Chi-85 in Figure S2a,c), the electrodes containing the crosslinked Chi-99-X and Chi-85-X (Figure 4c and Figure 4d, respectively) reveal a more compact surface without apparent cracks and holes, i.e., an enhanced coating homogeneity (see also Figure S2b,d for the comparative cross-sectional SEM analysis). In addition, the crosslinked analogues display an enhanced cohesion as confirmed by comparative qualitative peel tests, for which only a minor amount of coating could be removed using the adhesive tape compared to the non-crosslinked binder-based electrodes (Figure S3).

The improved electrode morphology and coating layer cohesion directly translates into better electrochemical performance (Figure 5). In fact, the cycling stability of both Chi-99-X and Chi-85-X is greatly enhanced after the crosslinking (compare Figure 5a with Figure 2a). Interestingly, Chi-85-X offers slightly enhanced initial capacity and substantially improved cycling stability, while for Chi-99-X both aspects are greatly enhanced. Nonetheless, the evolution of the dis-/charge profiles of Chi-99-X (Figure 5b) shows substantially lower capacities along cycling-even though the fading rate is essentially the same as for Chi-85-X. The superior performance of these latter electrodes is apparent also when subjecting the electrodes to elevated dis-/charge rates (Figure 5c,d). The performance improvement resulting from crosslinking the binder is evident only for relatively lower C rates (up to 2 C in case of Chi-99-X) while it is particularly pronounced for elevated dis-/charge rates, i.e., 3 C to 10 C, for Chi-85-X. This indicates that, in spite of the crosslinking, Chi-99 is not an

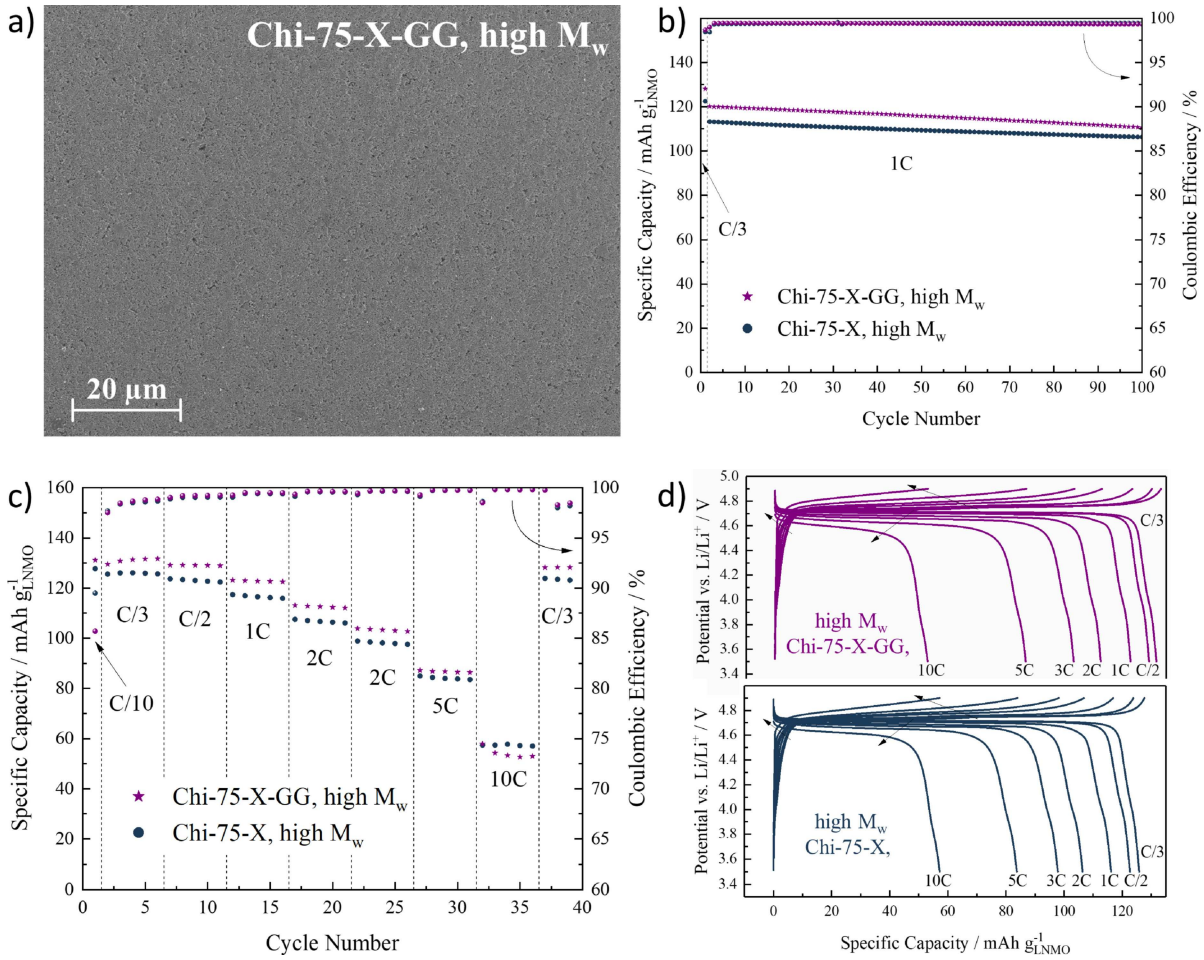

Figure 7. (a) SEM micrograph for high M_w Chi-75-X co-crosslinked with guar gum (GG; abbreviated: Chi-75-X-GG) as co-crosslinked binding polymer. (b) Constant current cycling for Chi-75-X-GG (purple) in comparison with Chi-75-X (dark blue). (c) Investigation of the rate capability for the two aforementioned electrodes and (d) selected potential profiles for these electrodes at different C rates. In all cases, the cut-off potentials were set to 3.5 and 4.9 V and a dis-/charge rate of 1 C corresponds to a specific current of 147 mA g^{-1}.

appropriate binder for the LNMO electrodes, which suffer significant polarization at elevated currents (Figure 5d). In contrast, Chi-85-X electrodes reach high and stable capacities, also at high dis-/charge rates, ascribable to their higher homogeneity and compactness (see Figure 4b,d).

Going to the high M_w chitosan binder (Chi-75), the electrode morphology looks much better already for the non-crosslinked electrode compared to the other two samples (Figure 6a compared to Figure 4a,b) with well-connected electrode components (Figure 6b). Nonetheless, also in this case the temperature-induced CA-crosslinking leads to improved morphology of the electrodes, which appear more densely packed and smoother (Figure 6c). The corresponding electrochemical data nicely reflects these morphological improvements of the Chi-75-X electrodes, which offer slightly improved cycling stability and higher capacities compared to the Chi-75 electrodes (Figure 6d).

In spite of such improvements, the Chi-75-X electrodes still suffer from being rather brittle upon mechanical deformation, which limits their active material mass loading and hampers their processability for large-scale production. In order to increase the solid content in the electrode slurry while improving the electrode flexibility, thus enabling higher active mass loadings, a second binding polymer was introduced to be co-crosslinked with chitosan. Towards this end, cheap and readily available guar gum was employed. This branched biopolymer is more flexible and well-capable of covering the active material more thoroughly thanks to the large amount of free hydroxyl groups forming hydrogen bridges,[55–58] helping to obtain mechanically stable electrodes with rather high active mass loadings.[59] In fact, crosslinking the blend of Chi-75 and guar gum (Chi-75-X-GG) yields electrodes with appropriate morphology (compare Figure 7a with Figure 6c) and high flexibility (Figure S4) in spite of the increased active material mass loadings (Chi-75-X-GG: 4.9 mg cm^{-2}; Chi-75–X. 3.3 mg cm^{-2}). Moreover, the Chi-75-X-GG electrodes provide further increased specific capacities at C rates up to 5 C-e.g., 131 mAh g^{-1} at C/3 and 123 mAh g^{-1} at 1 C compared to 126 mAh g^{-1} at C/3 and 116 mAh g^{-1} at 1 C for Chi-75-X (Figure 7b and 7c). Additionally, they display comparably little polarization as indicated by the 'manganese feature' appearing around 4.0 V (Figure 7d) despite the roughly 50% increased

mass loading. Only at dis-/charge rates as high as 10 C, the performance of Chi-75-X-GG is slightly inferior to that of Chi-75-X due to a slightly higher polarization, which can be simply assigned to the higher mass loading.

Conclusions

The investigation of three distinct chitosan powders provided valuable correlations between their structural properties and their suitability as binder for high-voltage LNMO cathodes. Low M_w chitosan samples (Chi-85 and Chi-99) provide comparably lower capacities and inferior cycling stability than high M_w chitosan. This is due to the incapability of the short-chained polymers to build up a dense and robust electrode structure. However, their performance can be substantially improved through citric acid-mediated crosslinking, leading to better cycling stability and rate capability. Nonetheless, a relatively lower DD (as in bio-derived Chi-85) is beneficial for the overall performance and cost, since high DDs as for artificial Chi-99 are very cost-intensive. Lowering the DD further while increasing the M_w (Chi-75) results in even better electrochemical performance especially after crosslinking with citric acid (Chi-75-X). This is accompanied by additional cost decrease since the shrimp-derived chitin needs less treatment to obtain the long-chained chitosan with low DD.[60,61] Co-cross-linking the cheapest chitosan together with guar gum results in improving the mechanical stability and flexibility of the LNMO electrodes, enabling higher active material mass loadings (increased by about 50 %) and specific capacities (i.e., 131 mAh g^{-1} at C/3 and 123 mAh g^{-1} at 1 C). These results clearly demonstrate the feasible use of environmentally friendly bio-polymers dissolved in water as binders for the realization of sustainable and high-performance positive electrodes for lithium-ion batteries.

Acknowledgement

The authors would like to acknowledge financial support from the German Federal Ministry of Education and Research within the Li-EcoSafe project (03X4636A & 03X4636D). The financial support from the Helmholtz Association is also acknowledged.

Conflict of Interest

The authors declare no conflict of interest.

Keywords: aqueous electrode processing · chitosan · binder crosslinking · high-voltage cathode · lithium-ion battery

[1] T. Nagaura, K. Tozawa, *Prog. Batteries Sol. Cells* **1990**, *9*, 209.
[2] Y. Nishi, *Chem. Rec.* **2001**, *1*, 406–413.
[3] A. Tovey, "Volvo becomes the first major car manufacturer to go all electric," can be found under https://www.telegraph.co.uk/business/2017/07/05/volvo-becomes-first-major-car-manufacturer-go-electric/, **2017**, accessed at March 20, 2019.
[4] P. A. Eisenstein, "GM Is Going All Electric, Will Ditch Gas- and Diesel-Powered Cars," can be found under https://www.nbcnews.com/business/autos/gm-going-all-electric-will-ditch-gas-diesel-powered-cars-n806806, **2017**, accessed at March 19, 2019.
[5] C. Hetzner, "BMW exec explains why automaker changed its electrification strategy," can be found under https://europe.autonews.com/automakers/bmw-exec-explains-why-automaker-changed-its-electrification-strategy, **2018**, accessed at March 19, 2019.
[6] M. Herdlitschka, C. J. Sedlmayr, K. Groeneveld, "Plans for more than ten different all-electric vehicles by 2022: All systems are go," can be found under https://media.daimler.com/marsMediaSite/en/instance/ko.xhtml?oid=29779739, **2017**, accessed at March 19, 2019.
[7] C. Pillot, *Avicenne energy* **2017**, 1–43.
[8] C. J. Barnhart, S. M. Benson, *Energy Environ. Sci.* **2013**, *6*, 1083.
[9] D. Larcher, J. M. Tarascon, *Nat. Chem.* **2015**, *7*, 19–29.
[10] S. Roberts, G. Gunn, in *Critical Metals Handbook*, John Wiley & Sons, **2013**, pp. 122–149.
[11] M. Li, J. Lu, Z. Chen, K. Amine, *Adv. Mater.* **2018**, *30*, 1–24.
[12] A. Kwade, W. Haselrieder, R. Leithoff, A. Modlinger, F. Dietrich, K. Droeder, *Nat. Energy* **2018**, *3*, 290–300.
[13] D. Bresser, D. Buchholz, A. Moretti, A. Varzi, S. Passerini, *Energy Environ. Sci.* **2018**, *11*, 3096–3127.
[14] K. P. Lee, N. C. Chromey, R. Culik, J. R. Barnes, P. W. Schneider, *Toxicol. Sci.* **1987**, *9*, 222–235.
[15] D. E. Malek, L. A. Malley, T. W. Slone, G. S. Elliott, G. L. Kennedy, W. Mellert, K. Deckardt, C. Gembardt, B. Hildebrand, S. R. Murphy, *Drug Chem. Toxicol.* **1997**, *20*, 63–77.
[16] W. Zhu, D. R. Schmehl, C. A. Mullin, J. L. Frazier, *PLoS One* **2014**, *9*, e77547.
[17] I. J. Davidson, S. Niketic, Y. Abu-Lebdeh, F. M. Courtel, D. Duguay, *J. Power Sources* **2010**, *196*, 2128–2134.
[18] K. Notake, T. Gunji, H. Kokubun, S. Kosemura, Y. Mochizuki, T. Tanabe, S. Kaneko, S. Ugawa, H. Lee, F. Matsumoto, *J. Appl. Electrochem.* **2016**, *46*, 267–278.
[19] T. Tanabe, T. Gunji, Y. Honma, K. Miyamoto, T. Tsuda, Y. Mochizuki, S. Kaneko, S. Ugawa, H. Lee, T. Ohsaka, *Electrochim. Acta* **2016**, *224*, 429–438.
[20] Q. Zhang, J. Mei, X. Wang, F. Tang, W. Fan, W. Lu, *Electrochim. Acta* **2014**, *143*, 265–271.
[21] Z. Karkar, D. Guyomard, L. Roué, B. Lestriez, *Electrochim. Acta* **2017**, *258*, 453–466.
[22] Z. Zhang, T. Zeng, Y. Lai, M. Jia, J. Li, *J. Power Sources* **2014**, *247*, 1–8.
[23] P. P. Prosini, M. Carewska, A. Masci, *Solid State Ionics* **2015**, *274*, 88–93.
[24] P. P. Prosini, M. Carewska, C. Cento, A. Masci, *Electrochim. Acta* **2014**, *150*, 129–135.
[25] A. Kazzazi, D. Bresser, A. Birrozzi, J. Von Zamory, M. Hekmatfar, S. Passerini, *ACS Appl. Mater. Interfaces* **2018**, *10*, 17214–17222.
[26] W. Y. Chou, Y. C. Jin, J. G. Duh, C. Z. Lu, S. C. Liao, *Appl. Surf. Sci.* **2015**, *355*, 1272–1278.
[27] F. Bigoni, F. De Giorgio, F. Soavi, C. Arbizzani, *J. Electrochem. Soc.* **2016**, *164*, A6171–A6177.
[28] J. Li, R. Klöpsch, S. Nowak, M. Kunze, M. Winter, S. Passerini, *J. Power Sources* **2011**, *196*, 7687–7691.
[29] I. Doberdò, N. Löffler, N. Laszczynski, D. Cericola, N. Penazzi, S. Bodoardo, G. T. Kim, S. Passerini, *J. Power Sources* **2014**, *248*, 1000–1006.
[30] Z. Wang, N. Dupré, A.-C. Gaillot, B. Lestriez, J.-F. Martin, L. Daniel, S. Patoux, D. Guyomard, *Electrochim. Acta* **2012**, *62*, 77–83.
[31] M. Dash, F. Chiellini, R. M. Ottenbrite, E. Chiellini, *Prog. Polym. Sci.* **2011**, *36*, 981–1014.
[32] M. Echetna, H. Ahlafi, F. Boukhlifi, S. My Slimane, H. Moussout, M. N. Bennani, *Mediterr. J. Chem.* **2013**, *2*, 503–513.
[33] G. A. F. Roberts, K. E. Taylor, *Makromol. Chem.* **1989**, *190*, 951–960.
[34] H. Gao, W. Zhou, J. H. Jang, J. B. Goodenough, *Adv. Energy Mater.* **2016**, *6*, 1–7.
[35] R. O. Beauchamp, M. B. G. St Clair, T. R. Fennell, D. O. Clarke, K. T. Morgan, F. W. Karl, *Crit. Rev. Toxicol.* **1992**, *22*, 143–174.
[36] Y. Zheng, D. Huang, A. Wang, *Anal. Chim. Acta* **2011**, *687*, 193–200.
[37] S. M. Gawish, S. M. Abo El-Ola, A. M. Ramadan, A. A. AbouEl-Kheir, *J. Appl. Polym. Sci.* **2011**, *123*, 3345–3353.
[38] X. Zhao, C.-H. Yim, N. Du, Y. Abu-Lebdeh, *J. Electrochem. Soc.* **2018**, *165*, A1110–A1121.
[39] K. Amine, H. Tukamoto, H. Yasuda, Y. Fujita, *J. Power Sources* **1997**, *68*, 604–608.

[40] M. Mancini, P. Axmann, G. Gabrielli, M. Kinyanjui, U. Kaiser, M. Wohlfahrt-Mehrens, *ChemSusChem* **2016**, 1843–1849.
[41] G. Gabrielli, M. Marinaro, M. Mancini, P. Axmann, M. Wohlfahrt-Mehrens, *J. Power Sources* **2017**, *351*, 35–44.
[42] S. Patoux, L. Daniel, C. Bourbon, H. Lignier, C. Pagano, F. Le Cras, S. Jouanneau, S. Martinet, *J. Power Sources* **2009**, *189*, 344–352.
[43] H. Zhong, J. He, L. Zhang, *Mater. Res. Bull.* **2017**, *93*, 194–200.
[44] H. Zhong, J. Lu, A. He, M. Sun, J. He, L. Zhang, *J. Mater. Sci. Technol.* **2017**, *33*, 763–767.
[45] M. M. Thackeray, M. M. Thackeray, M. M. Thackeray, *J. Am. Ceram. Soc.* **1999**, *82*, 3347–3354.
[46] G. E. Brown, V. E. Henrich, W. H. Casey, D. L. Clark, C. Eggleston, A. Felmy, D. W. Goodman, M. Grätzel, G. Maciel, M. I. McCarthy, *Chem. Rev.* **1999**, *99*, 77–174.
[47] N. Loeffler, G.-T. T. Kim, F. Mueller, T. Diemant, J.-K. K. Kim, R. J. J. Behm, S. Passerini, *ChemSusChem* **2016**, *9*, 1112–1117.
[48] M. Kuenzel, D. Bresser, T. Diemant, D. V. Carvalho, G. T. Kim, R. J. Behm, S. Passerini, *ChemSusChem* **2018**, *11*, 562–573.
[49] M. Y. Abeywardana, N. Laszczynski, M. Kuenzel, D. Bresser, S. Passerini, B. Lucht, *Int. J. Electrochem.* **2019**, *2019*, 1–7.
[50] P. Axmann, G. Gabrielli, M. Wohlfahrt-Mehrens, *J. Power Sources* **2016**, *301*, 151–159.
[51] R. M. Silverstein, F. X. Webster, D. Kiemle, *Spectrometric Identification of Organic Compounds, 7th Edition*, Wiley, **2005**.
[52] W. Porcher, B. Lestriez, S. Jouanneau, D. Guyomard, *J. Electrochem. Soc.* **2009**, *156*, A133.
[53] A. Manthiram, K. Chemelewski, E.-S. Lee, *Energy Environ. Sci.* **2014**, *7*, 1339.
[54] M. Mancini, G. Gabrielli, P. Axmann, M. Wohlfahrt-Mehrens, *J. Electrochem. Soc.* **2017**, *164*, A6229–A6235.
[55] B.-R. Lee, S. Kim, E.-S. Oh, *J. Electrochem. Soc.* **2014**, *161*, A2128–A2132.
[56] T. Zhang, J. Li, J. Liu, Y. Y. Deng, Z. Wu, Z. Z. Yin, D. Guo, L. Huang, S.-G. Sun, J. Li, *Chem. Commun.* **2016**, *52*, 4683–4686.
[57] J. Liu, Q. Zhang, T. Zhang, J. T. Li, L. Huang, S. G. Sun, *Adv. Funct. Mater.* **2015**, *25*, 3599–3605.
[58] M. K. Dufficy, S. A. Khan, P. S. Fedkiw, *J. Mater. Chem. A* **2015**, *3*, 12023–12030.
[59] D. V. Carvalho, N. Loeffler, M. Hekmatfar, A. Moretti, G. T. Kim, S. Passerini, *Electrochim. Acta* **2018**, *265*, 89–97.
[60] Sigma-Aldrich, "Chemicals: Natural Polymers and Biopolymers, Chitosan (Animal Origin)," can be found under https://www.sigmaaldrich.com/materials-science/material-science-products.html?TablePage=112230133, **2019**, accessed at April 18, 2019.
[61] I. Younes, M. Rinaudo, *Mar. Drugs* **2015**, *13*, 1133–1174.

Manuscript received: September 30, 2019
Revised manuscript received: October 22, 2019
Accepted manuscript online: October 23, 2019
Version of record online: November 12, 2019